ELSEVIER

Cryogenics 43 (2003) 179–197

Cryogenics

www.elsevier.com/locate/cryogenics

Analysis and interpretation of the full set (2000–2002) of T_{CS} tests in conductor 1A of the ITER Central Solenoid Model Coil

R. Zanino [a,*], N. Mitchell [b], L. Savoldi Richard [a]

[a] *Dipartimento di Energetica, Politecnico di Torino, c. Duca degli Abruzzi 24, I-10129 Torino, Italy*
[b] *ITER IT, Naka 311-0193, Japan*

Received 18 September 2002; accepted 14 January 2003

Abstract

The full set of T_{CS} measurements performed during 2000–2002 on conductor 1A of the ITER Central Solenoid Model Coil (CSMC) of the International Thermonuclear Experimental Reactor (ITER) is analysed with the extensively validated M&M code. Under the assumptions of uniform strand properties and uniform current distribution among strands, the performance of this "average" strand in the cable is deduced from the best fit of the measured voltage–inlet temperature characteristics. Two fitting parameters are chosen: an ad-hoc additional contribution 'ε_{extra}' to the longitudinal strain of the average strand in the cable, and the average-strand (or cable "effective") index 'n' of the electric field–current density characteristic. It is shown that the average strand in the CSMC performed less well than expected from the strand database—an increasingly negative ε_{extra} being needed to reproduce the coil behaviour at increasing transport currents, and that the cable effective n is clearly below the measured n of the strand. It is argued that this average-strand performance reduction in the CSMC is most likely related to mechanical load effects.

Keywords: Cable in conduit conductors; Superconductors; Supercritical helium; Current sharing; Fusion magnets

1. Introduction

The International Thermonuclear Experimental Reactor (ITER) central solenoid model coils [1,2] consist of the Central Solenoid Model Coil (CSMC) and three associated insert coils, the Central Solenoid Insert (CSI) and the Toroidal Field Insert (TFI), which both use a Nb_3Sn conductor, and the Aluminium Insert (ALI), which uses a Nb_3Al conductor. The CSMC and associated inserts produce a high field (~13 T) and were designed to qualify the full-size ITER conductors at and beyond the ITER operating conditions, by providing a long length of conductor at high field. The stored energy of the system is about 640 MJ.

The CSMC is a layer wound coil, using a thick 'circle in square' type of jacket made of a low coefficient of expansion (COE) material, Incoloy 908, with a kapton–glass–epoxy insulation system. It is wound as two-in-hand layers with joints at top and bottom, and the length of each unit of the innermost layer is about 80 m. The layout of the coil is shown in Fig. 1. Layer 1A, the subject of this paper, is one of the two conductor units forming the innermost layer of the inner module.

The conductor in the coils is the well-known 'cable-in-conduit' (CICC) type where a multistage cable of 1152 strands is contained in a conductor jacket. The cable is built up typically in a $3 \times 4 \times 4 \times 4 \times 6$ combination of subunits, with the basic starting unit a triplet of three strands and the final cable made up of six sub-stages twisted around a central channel, each with a thin wrap of Inconel foil [1]. Helium flows in the central channel and in the annulus, around the strands. The maximum operating current is 46 kA for the CSMC, at which point the field is about 13 T in the inner bore. Field maps of the coil and the innermost layer are shown in Fig. 2.

Testing of the coils is complete, with three test campaigns since 2000 on the CSMC and Inserts lasting a total of about five months. Altogether, the CSMC has undergone about 150 charge–discharge sequences to currents over 30 kA and Layer 1A has experienced at least four quenches, plus three complete cooldown–warmup cycles to 300 K.

* Corresponding author. Tel.: +39-011-564-4490; fax: +39-011-564-4499.
E-mail address: zanino@polito.it (R. Zanino).

0011-2275/03/$ - see front matter
doi:10.1016/S0011-2275(03)00035-3

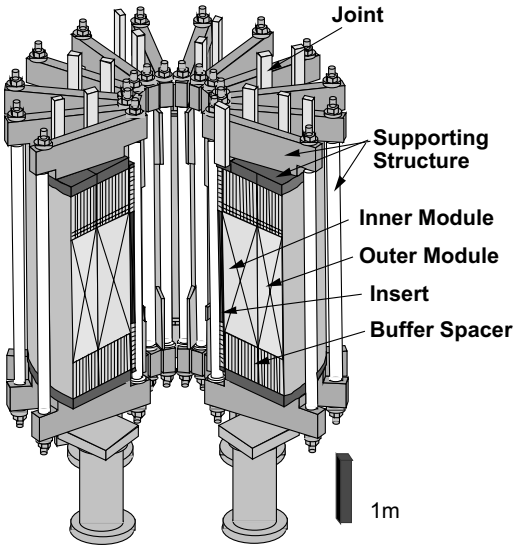

Fig. 1. The CSMC and Insert coil.

The cable-in-conduit (CIC) design was selected for ITER because of its potential high stability under transient conditions, as well as low manufacturing costs. The helium flowing around the strands provides good cooling. At the same time, controlled strand-to-strand contact resistance (by suitable selection of compaction and coating) allows non-uniform currents to redistribute within the cable while limiting AC coupling currents. As far as the steady state performance is concerned, it is necessary to ensure that the conductor operating point in ITER is far enough from the point where resistive current sharing develops, to avoid the possibility of a runaway quench. One of the objectives of the CSMC tests was to measure the current sharing behaviour of the conductor and compare it with predictions based on measurements of the strand properties used to make it. Having done this, we can derive design criteria (such as those given in [3]) that ensure that the strand data is applied in such a way that the conductor will operate in ITER with adequate margins. Of course, the use of excessive margins carries a very high cost and space penalty (the Nb_3Sn strands represent about 8% of the total machine cost) and the margins must be kept to a minimum. This requires an accurate and complete understanding of the processes associated with the strand performance in a conductor.

Measurements on the CSMC have consisted of:

(i) Current sharing temperature (T_{CS}) measurements at constant current with slow ramped temperature on the highest field layer;
(ii) Joint resistance measurements and pulse stability assessment, on all joints;
(iii) Ramp-rate tests (increasing and decreasing current on a timescale of 20–30 s to full current);
(iv) AC coupling loss measurements on all layers.

In contrast to the case of AC loss data, where all layers are heated more or less to the same temperature, it is very difficult to extract the conductor performance from the T_{CS} measurement data, since in these tests only two layers are heated (see below), leading to the appearance of thermal gradients in the coil, both along a conductor and across the winding pack between different conductors.

Only overall conductor voltage measurements are available. To interpret these data, a matching overall voltage evolution has also to be calculated from the evolution of the local electric field distribution along the conductor, but this requires fairly accurate predictions of both the local temperature and the local strain along

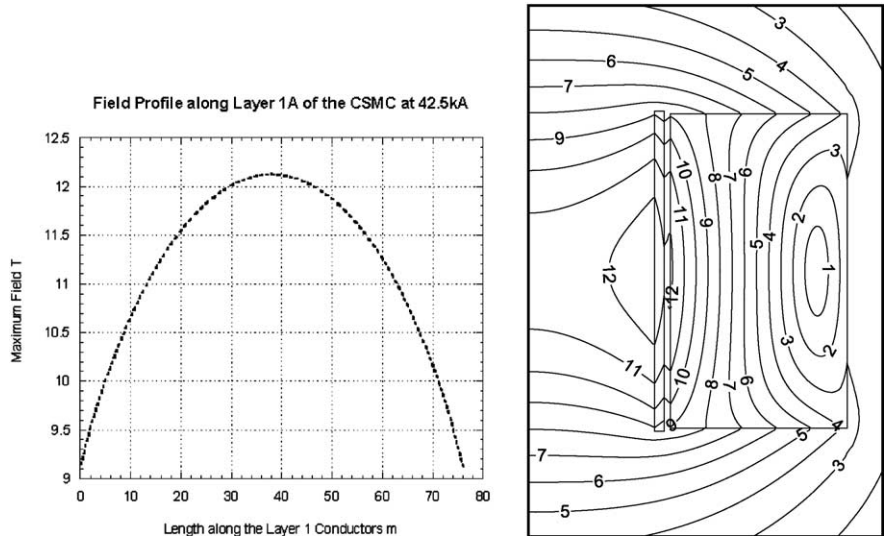

Fig. 2. Field maps for the CSMC with 42.5 kA in the CSMC and 40 kA in the CSI (magnetic field in T).

the conductor. The deduction of the strand performance in the conductor then requires iterations with the thermal calculations to deduce appropriate performance values for the strand in the conductor that fit all the thermal and overall voltage data.

Some of the factors that must be considered for this deduction (such as the treatment of conductor transverse field gradients) are discussed in the next section. However, one factor relates to the overall method of interpretation. Nb_3Sn is well known to have strain-sensitive superconducting properties (critical current, field and temperature). One of the main 'steady state' design issues is the identification of the strand strain states inside the conductor. On a simple '1D' basis, this is a combination of the operating strain of the conduit (which is stretched as it reacts the coil magnetic bursting pressure) and the differential thermal contraction between cable and jacket. On a multidimensional basis, the cable is a mass of bent strands, locally unsupported for short lengths, and both the local magnetic forces on individual strands (acting transversely but creating longitudinal stresses), and three-dimensional deformation under the longitudinal operating plus thermal strains, can complicate the situation. We will summarise the overall cable performance by deriving the equivalent longitudinal strain state of the strands in it, defined here as $\varepsilon_{\text{total}}$, using the parametric representation of the strand properties described later. For interpretation purposes we split the strain into three components as described above, a thermal component $\varepsilon_{\text{thermal}}$, a longitudinal strain due to the operating strain (on the jacket) ε_{op}, and an ad-hoc extra longitudinal component (which may contain contributions from both thermal and operating strain, see below):

$$\varepsilon_{\text{total}} = \varepsilon_{\text{thermal}} + \varepsilon_{\text{op}} + \varepsilon_{\text{extra}}.$$

ε_{op} is often known from stress analysis (see below). The expected thermal strain $\varepsilon_{\text{thermal}}$ in the cable, due to the differential thermal contraction between Nb_3Sn filaments and Incoloy jacket from the reaction heat treatment, is taken as -0.32%, based on measurements of sub-size Incoloy conductors in the Specking FBI facility at Forschungszentrum Karlsruhe (FZK) [4]. This value also corresponds to that predicted by a fully bonded model which considers the differential thermal contraction of the cable and jacket from the reaction heat treatment temperature.

In the past, the first set of CSMC T_{CS} measurements was already analysed with the M&M code [5,6], with particular emphasis on the thermal-hydraulic aspects involved in modelling the complex cryogenic circuit of the whole winding. More recently, a simplified thermal-hydraulic model was used for a first assessment of possible degradation of performance in the CSMC based on the analysis of voltage–temperature characteristics [7], and M&M was applied to a comparative analysis of the 2000 and 2001 T_{CS} measurements at maximum current (46 kA) [8]. The same tool and strategy was also very recently applied to the assessment of the ITER Toroidal Field Model Coil (TFMC) standalone (Phase I) performance [9,10], based on the analysis of the T_{CS} tests performed at FZK.

The present paper is organized as follows: the test procedure for the T_{CS} measurements is presented first. A critical discussion of the input data for the analysis is then given, with particular reference to the strand database. The M&M model is then shortly reviewed, and applied to the analysis of the full set of T_{CS} tests. The implications of the analysis for the evaluation of the CSMC performance are finally discussed and conclusions are drawn.

2. Test procedure

All T_{CS} tests on layer 1A of the CSMC have been performed using the same procedure. After the ramp-up of the current, the helium at the inlet of conductor 1A is heated in steps (which become smaller as the temperature gets closer to the foreseen T_{CS} value) by means of resistive heaters wound around the helium pipe at the common inlet of the first two layers. This proceeds until a voltage of $\sim$0.2–0.5 mV, estimated to roughly correspond to the T_{CS} definition $E = E_{\text{C}}$ (electric field equal to its critical value), develops on one of the innermost conductors (typically 1A). Then the current dump was started, avoiding in most cases the quench of the coil (see below).

Since a strong thermal coupling was foreseen, both between conductors in the same layer and between conductors in adjacent layers [11], which are all hydraulically in parallel, the heater location was aimed at minimizing the temperature gradient along conductor 1A, see Fig. 3. Despite that, a significant heat transfer is still present in the inlet joint between conductor 1B and the inter-module busbar [12], and between conductor 2A and 3B, so that after the inlet joint the helium in 1B and 2A is colder than that in the other two heated conductors [6]. Therefore, even within the two heated layers, heat transfer effects are important.

The major characteristics of the full set of T_{CS} tests performed during 2000–2002 on conductor 1A of the CSMC are summarized in Table 1. As the power available from the heaters is limited, during the T_{CS} tests the mass flow rate in the first two layers was reduced from the nominal 10 g/s using the valve at the common outlet, to allow a high enough temperature to be reached in 1A. The variation in mass flow rate between the layers also complicates the comparison of the results for otherwise nominally identical measurements.

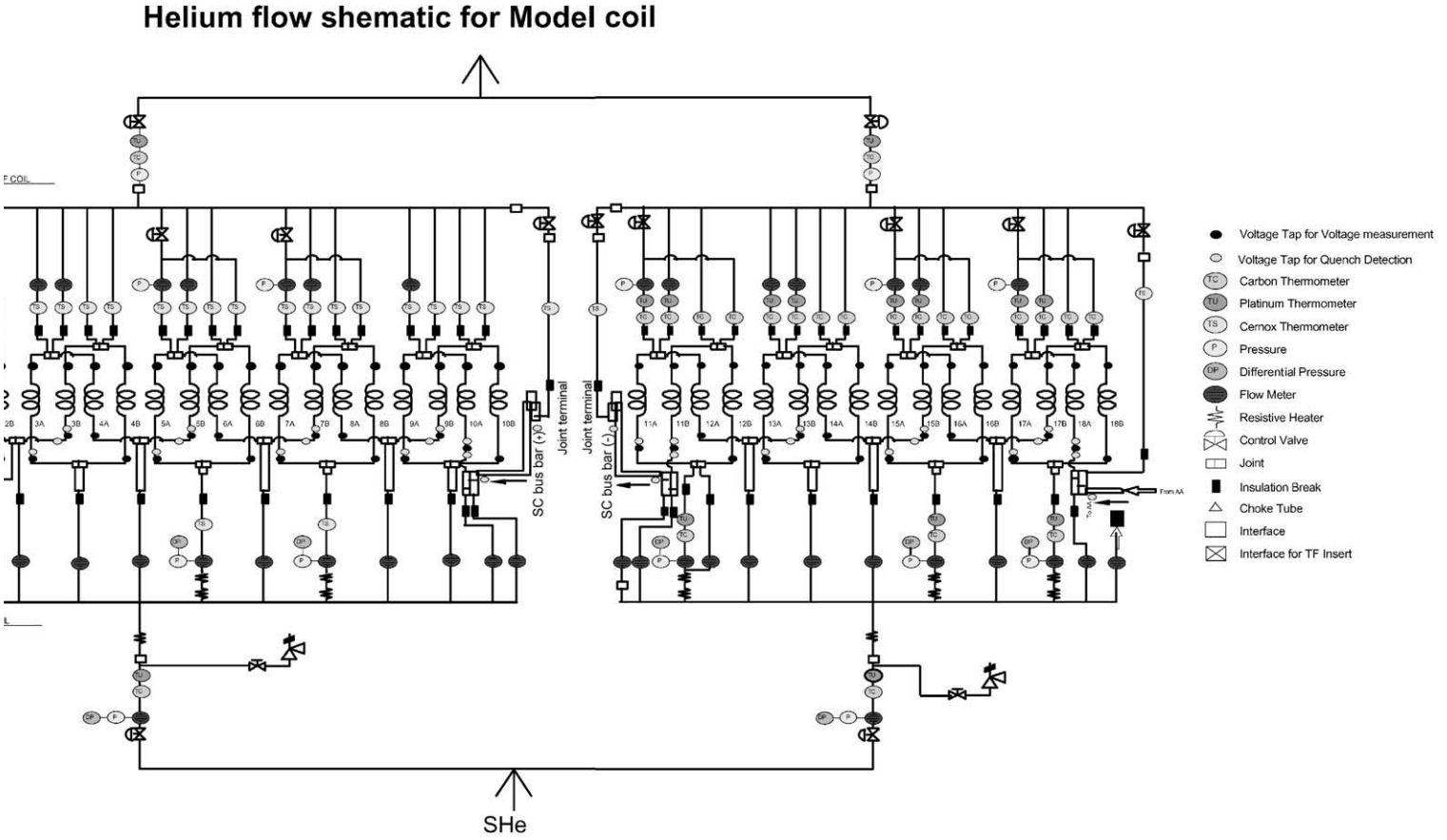

Fig. 3. Schematic of the CSMC hydraulic circuit. Helium flow is from bottom to top. Notice the heaters on the inlet plumbing common to conductor 1A, 1B, 2A, 2B, the joints (open rectangles), and the location of the temperature (TS), pressure (*P*) and flow sensors. The small black circles are the voltage taps. The "from A"–"to AA" branch cools the inter-module busbar connecting the innermost layer of the inner module to the outermost layer of the outer module.

Table 1
Summary of the T_{CS} tests performed on CSMC conductor 1A

Current (kA)	Shot #	Year	Total test duration[a] (s)	Initial mass flow rate in 1A (g/s) (inlet–outlet)	Comments
46	038-002	2000	~15000	4.0–4.2	
	020-002	2001	~7100	5.0–5.6	
	089-002	2001	~7000	4.9–5.2	
	090-002	2002	~6900	5.1–5.3	
40	041-002	2000	~9100[b]	4.1–4.5	Quench in layer 1
30	051-002	2000	~11000[c]	3.0–3.7	
	092-002	2002	~13000	3.3–3.0	
20	094-002	2002	~13000	2.9–3.2	Quench in layer 2
1	055-001	2000	~10000	3.0–2.0	Not analysed with M&M

[a] From the initial temperature of ~4.5 K.
[b] From the initial temperature of ~6.5 K.
[c] From the initial temperature of ~7.2 K.

3. Input data for the analysis

The CSMC 1A conductor uses Vacuumschmelze strand with cabling by EM-LMI. Jacketing was performed by Ansaldo using Incoloy 908 CS tubes from Inco Alloys. The main parameters are summarised in Table 2.

The strand data is based on measurements performed on isolated strands, as a function of temperature, field and in a few cases applied strain. Various empirical parametric scalings are conventionally used to fit Nb_3Sn data and, in this paper, Summers' formula [13] is used. This allows the strand critical current to be derived once three characteristic parameters are defined, C_0, T_{c0m} and B_{c20m}, and the strain is known. Conversely, if the strand performance in the cable is known, the expression allows the effective strand strain to be derived.

The accuracy of the Summers scaling can be a concern when it is applied over a large range, particularly when not supported by critical current measurements as a function of strain. For the CSMC this is not so significant as the isolated strand intrinsic strain is already close to the cable operating strain, and the main operating range (10–13 T and 6.5–11.5 K) is well covered by strand characterisation measurements. Ref. [12] provides an assessment of the fitting error for the Summers scaling when a least squares method is used to determine the best parameters fitted to the CSMC layer 1A strand data measured over the range 0–20 T and 4.2–11 K, without any externally applied strain. The error in critical current between measured and predicted values can approach 30% using this procedure. However, as will be seen below, restricting the range of the fit greatly improves the accuracy.

Table 2
Strand, cable and conductor parameters in the CSMC layer 1A

Strand diameter	0.81 mm
Cu:non-Cu ratio	1.5
Coating	2 μm Cr
Strand type	Nb_3Sn bronze
Cable build	$3 \times 4 \times 4 \times 4 \times 6$
Central cooling tube	12 mm (OD), 10 mm (ID)
Cable OD	38.5 mm
Conductor dimensions	51 mm × 51 mm

Measurements of the strand performance are available from the following sources:

(i) University of Twente measurements on both strained and unstrained strands [14,15]. These measurements are not evaluated in terms of the Summers formula but with an improved parametric scaling which gives a much better fit to the measured data over the whole measurement range. Some data (without applied strain) is measured at the standard electric field of 10 μV/m, but the strained strand measurements are made at 500 μV/m (due to the short specimen length) and need to be treated with caution.
(ii) CEA Cadarache extended measurements up to 20 T [16], without applied strain. This report provides derivations of the Summers parameters.
(iii) ITER JCT assessments of the CSMC conductor strand average performance based on the strand QA data at 12 T and 4.2 K supplied by the manufacturers [17].
(iv) Measurements on witness strands co-reacted with layer 1 [18] and measured at 12 T, 4.2 K.
(v) Strand characterisation performed at Durham University [19] on strained strands. As with (i), this report does not use the Summers scaling to fit the strand data, but develops another, improved, scaling method. The object of this work was to characterise the strand as a function of strain. Due to

the type of sample holder, there are no measurements on isolated strands without an applied strain, which prevents a straight comparison with the QA data. However the strain data is measured with the standard 10 μV/m criterion. Detailed comparisons with the data from (i) show good agreement over the full field-temperature–strain measurement range.

(vi) FZK measurements on short (straight) strands under applied tension in the FBI facility [20].

The VAC strand changed slightly over the duration of the supply due to improvements in the production method. Strands supplied for the various measurements above were not identical and this contributes to the variations described below. To illustrate this, Fig. 4 shows the critical current density (j_C) distribution in each of the 1152 strands making up the Layer 1A conductor.

The thermal strain of the filament in an isolated strand is needed to determine the strain at which the critical current measurement applies. Source (i) gives a thermal strain of −0.22% for an isolated strand and source (vi) gives −0.23% (measured at an electric field of 100 μV/m instead of the conventional 10 μV/m). For comparisons between the parametric scalings recommended for the CSMC layer 1A and the strand data, a value of −0.22% has been used.

Source (ii) suggests that B_{c20m}, T_{c0m}, C_0 have values for the Summers' scaling of $B_{c20m} = 32.5$ T, $T_{c0m} = 16.35$ K, $C_0 = 0.71 \times 10^{10}$ A/m$^2\sqrt{\text{T}}$.

This data corresponds to a strand critical current density of 550 A/mm^2 at 4.2 K and 12 T (and 10 μV/m). The error of this scaling for the critical current, when compared to the unstrained strand data in (i) and (ii), appears quite high (>20%) in the CSMC layer 1A operating region (i.e. 10–13 T, 6.5–11.5 K) and needs to be reduced. At zero field and current, these scaling parameters also give an unacceptable error of >1 K when compared with very detailed measurements from source (i).

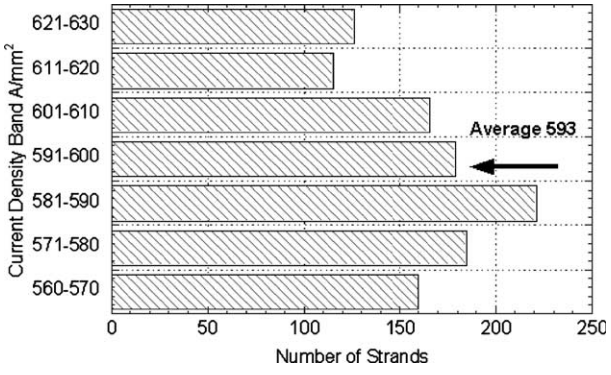

Fig. 4. Distribution of strand critical current density in layer 1A of CSMC (supplier data at 12 T and 4.2 K).

The average j_C at 12 T and 4.2 K using the strand QA documents (supplied by the manufacturer) is 593 A/mm^2 (source (iii)). It is known from the strand benchmark tests that the strand sample holders used by the manufacturer tend to stretch the strand and overestimate the j_C by several percent. The recommended correction value from the various benchmark actions is a 3% reduction to be applied to source (iii).

However, the measured data from source (iv) give a j_C about 9% less than the QA data supplied by the manufacturer. This is partly due to the type of sample holders used by the manufacturer, but the discrepancy between the 3% above and the 9% here has not been fully resolved. It is possibly due to differences in the actual heat treatment of the coil compared to that specified by the manufacturer (due to the need to outgas the cable during the temperature ramp up) and used for the QA measurements. The average strand critical current density from (iv) is about 557 A/mm^2 at 4.2 K and 12 T.

The critical current data from both (i) and (v) is in the range 550–560 A/mm^2 for 'unstrained' strand at 12 T and 4.2 K, at 10 μV/m. The measurement from (vi) is rather low, giving 500 A/mm^2 at 10 μV/m, although this is probably due to the limited accuracy of the measurement, due in turn to the short length of strand involved (5 cm). This measurement will be disregarded.

After some iterations, the parameter set finally used in our analysis was:

$$B_{c20m} = 32.0 \text{ T}, \quad T_{c0m} = 17.5 \text{ K},$$
$$C_0 = 0.74 \times 10^{10} \text{ A/m}^2\sqrt{\text{T}},$$
$$\text{strand strain} = -0.22\%,$$

which gives a strand critical current density of 590 A/mm^2 at 12 T and 4.2 K. As will be seen in the next paragraph, this parameter set tends to produce an overestimate of the critical current measured in the strands at 4.2 K and 12 T (by about 10%). However, within the CSMC measurement range (6.5–11.5 K and 10–13 T) it gives a much better fit, within ±25 A/mm^2 on critical current or ±0.1 K on current sharing temperature up to 10 K, to the strand data. In other words, despite an overestimate at 12 T and 4.2 K, in the CSMC operating range these parameters give a good match to strand data (source (i)) that at 12 T and 4.2 K give a critical current of about 540 A/mm^2.

Fig. 5 shows the fit produced by this scaling to some of the measured data (from [15] for unstrained strands). Although there is some overestimate of the critical current at low temperatures (about 10% at 4.2 K), in the CSMC operating range the fit is very good. Up to 10 K, the match to the critical current data is within 5%. At low strand currents this error increases to 10% at 11 K. The difference is systematic, with the parametric fit slightly overestimating the measurements. This reflects

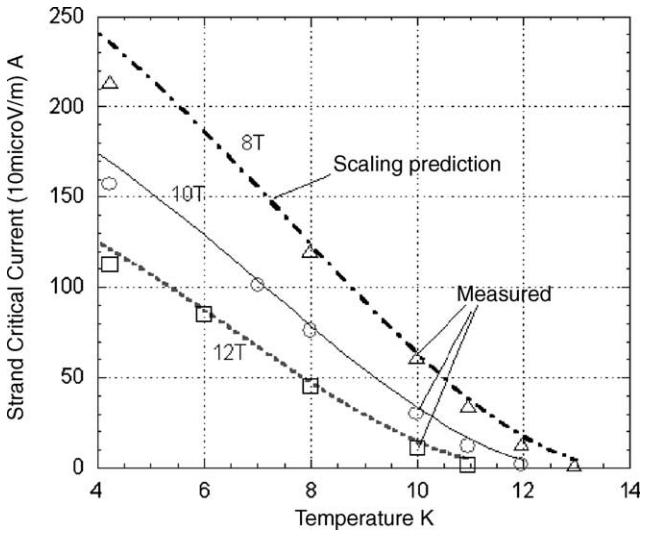

Fig. 5. Comparison of measured strand data (Twente University) with Summers' scaling $T_{c0m} = 17.5$ K, $B_{c20m} = 32.0$ T, $C_0 = 0.74 \times 10^{10}$ A/m$^2\sqrt{\text{T}}$, $\varepsilon_{th} = -0.22\%$.

the slight difference between the strand witness samples (source (iv)) and the more detailed measurements on individual strands, i.e., the actual error on the fit to the cable average critical current performance appears to be within $\pm 5\%$ in the CSMC operating range up to about 10 K. Expressed as an error in the current sharing temperature, this is about ± 0.1 K. The absolute critical current error at low currents (10–11.5 K) stays about the same, but the percentage increases. However, at low currents, the error on the current sharing temperature is more significant than the error on the critical current, and the figure shows that this remains within about ± 0.15 K. Comparison between the strand data and the scaling at very low current and field is included in the results and analysis section but shows the same error bar range in current sharing temperature.

A further property of the strands is the 'n_{strand}' value, used to measure the steepness of the transition from superconducting to normal conditions. This transition is found empirically to fit a curve of the form:

$$E = E_C (I/I_C)^{n_{strand}}$$

where E is the electric field, and E_C (usually 10 μV/m) is the field when the current I is equal to the critical value I_C.

The parameter n_{strand} is well established as a 'quality factor' for single strands, as low values tend to indicate non-uniform or broken filaments. It is also known to be affected by non-uniform strains over the strand cross-section [21]. Although the value of n_{strand} is not directly required for the present analysis, it is of importance for comparison with the 'effective' n for the cable produced by the interpretation (see below). n_{strand} is frequently quoted at 12 T and 4.2 K but is known to be a function of critical current and strain (i.e., dependent on temperature and field mainly through the critical current). For the VAC strand, n_{strand} at these conditions is about 20 [14–16,19]. More data on the n_{strand} value of the VAC strand is given in Section 6.

3.1. Operating strain

In the conductor, the operating strain distribution along the length is taken as

$$\varepsilon_{op} = (I_{CSMC}/46)^2 (0.0011 + 0.0005 s/L)/0.8275$$

where I_{CSMC} is the model coil current in kA, s (varying between 0 and $L/2$) is the distance measured from one end of the conductor, and L is the total conductor length (about 80 m), both measured along the conductor axis. The variation is symmetric about the conductor mid point and full bonding between jacket and cable is assumed. A peak operating strain of $\sim 0.16\%$ is predicted on the equatorial plane at peak current (46 kA).

The operating strain on the conductor was first estimated in the design phase of the coil from finite element stress analysis [22]. The expression above for ε_{op} was obtained by ad-hoc modification of the results of the analysis, in order to match them with the few measurements available from the coil in operation [23], which gave lower strain than expected.

3.2. Magnetic field

The field on the CSMC was calculated numerically [24] using a cable model with six circular petals. The maximum field on the CSMC is 0.285 T/kA, which gives 13 T at 45.58 kA. The calculations also include the field gradient across the conductor (i.e. moving in a radial direction), which is required to calculate the average electric field (see below). The total field change across the conductor at the maximum field point is 0.0236 T/kA. The variation of field along the conductor length is shown in Fig. 2.

The field contribution B_{inc} from the Incoloy has been calculated numerically [25]. The vertical field is increased inside the cable space and varies in both vertical and horizontal (radial) directions. The variation in the vertical direction is approximated by a constant value. The expression $B_{inc} = 0.075(r/r_{cable})^2 + 0.075$ T is used to approximate for the horizontal variation of the Incoloy field, where r is the distance in the horizontal direction measured from the centre of the cable, and r_{cable} is the total cable radius (19 mm). This field contribution is fixed for all external fields over 2 T, once the Incoloy saturates.

4. M&M model

The M&M model is the multi-conductor version of the Mithrandir model. Mithrandir was originally developed

to overcome the shortcomings of previous models where the same thermodynamic state was assumed for the helium in the central channel and in the cable bundle region of the dual-channel CICC typical of all ITER conductors. Mithrandir was validated against stability, quench and heat slug propagation data from the QUELL experiment and, more recently, against stability, quench and AC loss data of the ITER CSI coil [26–28] and against quench data of the ITER TFI coil [29].

In the model coils, however, the possibly strong heat transfer between the conductors in different layers or pancakes, or even between different conductors in the same layer, see Fig. 6, can have important effects on the temperature profile established along a given conductor, and a sometimes dominating effect is that of the heat transfer through the joints. The M&M model was thus developed to be able to deal with these effects in real coils [5]. Heat generation in and transfer through the joints were validated against dedicated experiments in the full size joint sample (FSJS) [30] and US prototype (USP) joint sample [12] tests. Therefore, we still need here to validate only the effect of inter-turn and inter-layer heat transfer in the CSMC (see below), before applying M&M to the analysis of voltage–inlet temperature (V–T_{in}) characteristics. In this respect it should also be emphasized that the absence of temperature measurements *inside* the CSMC makes it impossible to derive a V–T_{local} characteristic. We have therefore to compare computed and measured V–T_{in} characteristics, and rely on the accuracy of the validated code to reproduce the correct temperature profile along the conductor and therefore the corresponding E field distribution and resulting total resistive voltage drop. In view of the above-mentioned long list of successfully completed validation exercises, we claim that the M&M code is, to-date, the most extensively validated tool for the analysis of the ITER model coils, within the limitation of a uniform current distribution assumption.

Heat transfer in M&M accounts for all available paths in the CSMC, as shown in Fig. 6. In this paper, we simulate the first three layers of the inner module + the inter-module busbar, considering this set to be adiabatic to the rest of the coil. Based on previous work [11], this should be enough to obtain accurate temperature profiles in the innermost layer 1, which is both the warmest and the one at highest field, and as such the most likely to reach T_{CS} first.

Friction factors in M&M distinguish between the central channel's f_H and the bundle's f_B. For the former we use a correlation we developed in the past [31]. For f_B we use Katheder's correlation corrected with a multiplier of 1.35 [32]. The combination of these two recipes was already validated for the CSMC [33].

Finally, the average local electric field $\langle E \rangle(x)$ is computed as an average over the CICC cross section, assuming a linear magnetic field profile across it, based on average and peak magnetic field maps [24], according to the following formula:

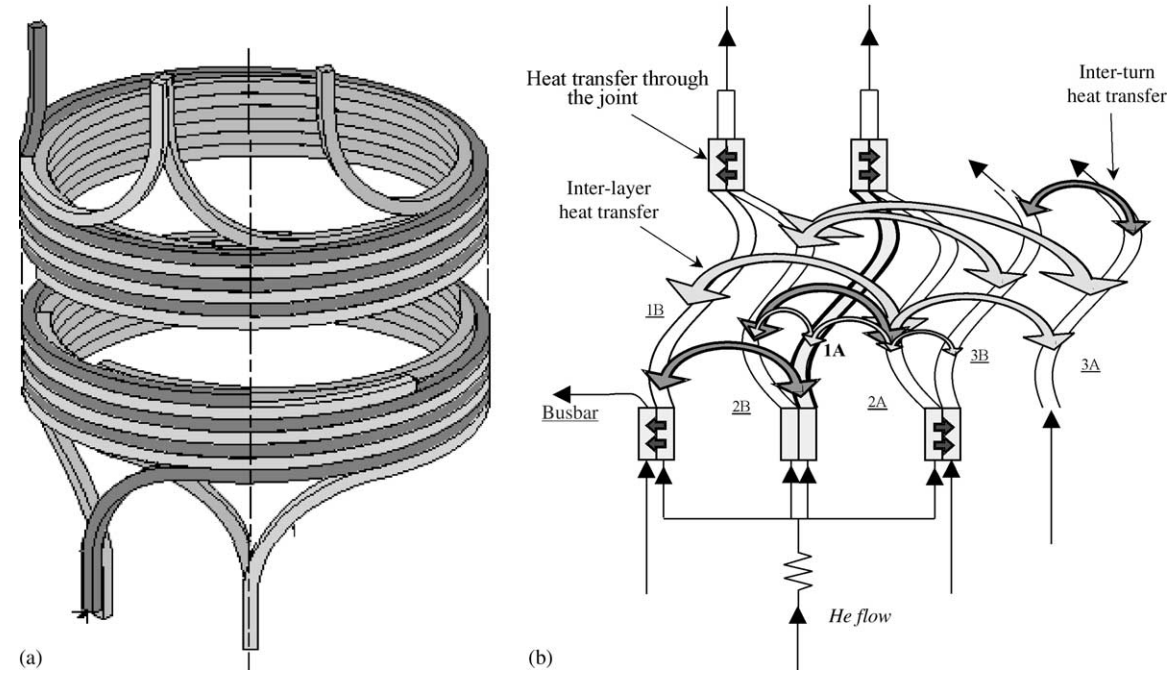

Fig. 6. (a) Artistic view of the topology of the first two CSMC layers (courtesy of Y. Nunoya). (b) Schematic view of the heat-transfer paths affecting the behaviour of conductor 1A.

$$\langle E\rangle(x) = \frac{2E_C}{\pi(R_{out}^2 - R_{in}^2)}\left[\int_{-R_{out}}^{R_{out}} (j/j_C(x,y))^n \sqrt{R_{out}^2 - y^2}\,dy - \int_{-R_{in}}^{R_{in}} (j/j_C(x,y))^n \sqrt{R_{in}^2 - y^2}\,dy\right]$$

where x is the coordinate along the conductor, y is the dummy variable indicating the coordinate across the conductor cross section, j is the operating current density (assumed to be uniform), R_{in} is the inner radius of the cable region (i.e., the outer radius of the spiral around which the cable is wound in a dual channel conductor), and R_{out} is outer radius of the cable region (i.e., the inner radius of the jacket). $\langle E\rangle$ is then integrated along the whole conductor length to obtain the voltage V.

We now proceed to the validation of the inter-turn and inter-layer heat transfer models against CSMC data. Based on experimental inlet temperatures and mass flow rates (which are used as boundary conditions everywhere in this paper) we compare the computed outlet temperature evolution in shots 038-002 and 051-002 with the corresponding measured values in the two innermost (directly heated) layers. The results of this comparison, shown in Fig. 7, indicate that the code is able to predict the outlet temperatures in layer 1 with an error of at most ± 0.1 K, when the Joule heating due to

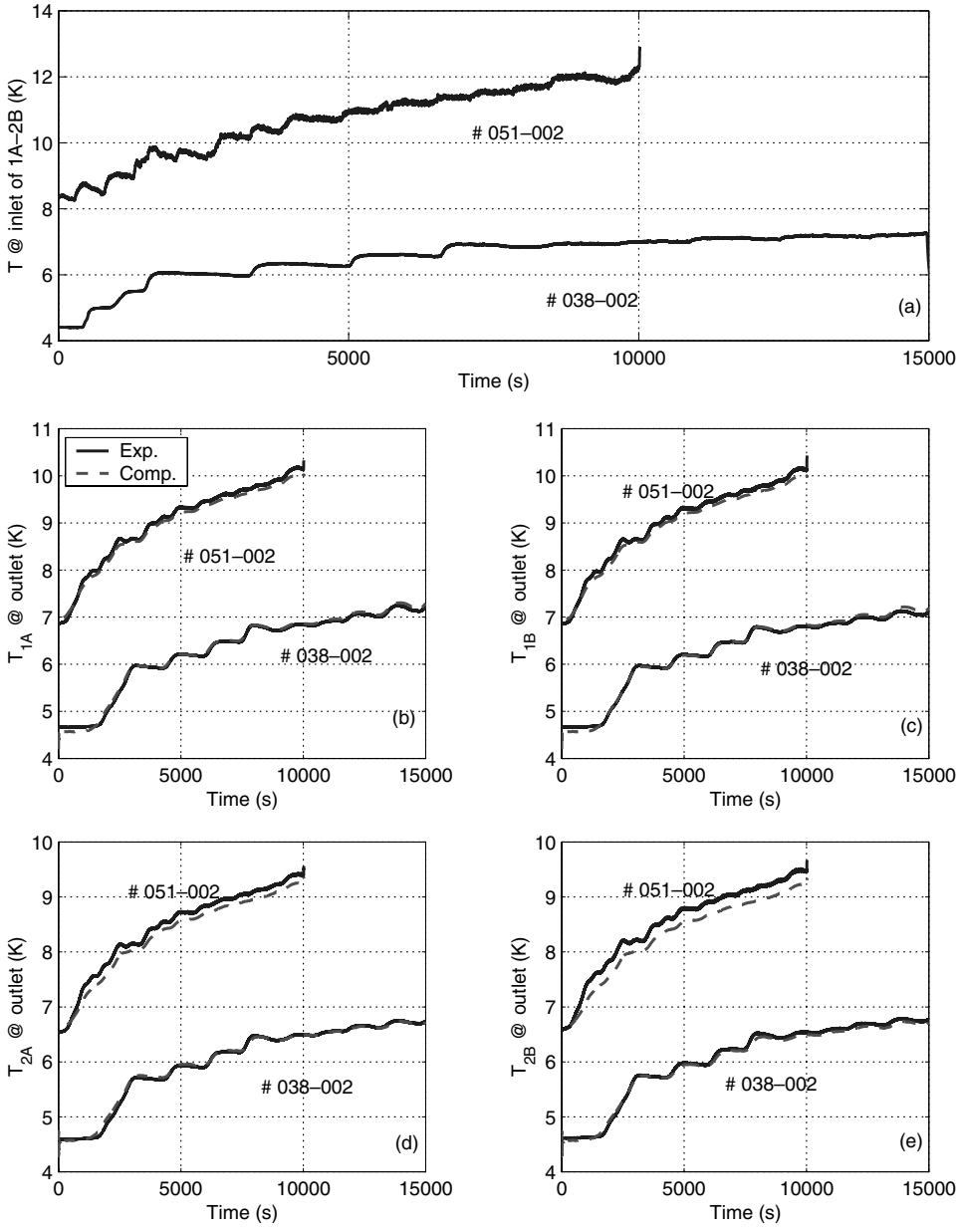

Fig. 7. The solid lines represent the evolution of the measured inlet (a) and outlet (b–e) temperature in the first two layers, for shot # 038-002 (46 kA) and shot # 051-002 (30 kA). The computed values (dashed) are also reported for comparison.

current sharing is negligible. Similar accuracy is found up to an inlet temperature of ~14 K (test at 20 kA), i.e., for a temperature difference of ~4 K between inlet and outlet of the conductor.

5. Experimental results and analysis

The evaluation of the experimental results will be done here mainly in terms of the V–T_{in} characteristic, in particular searching for the values of the parameters n and ε_{extra}, which allow, using M&M, a best fit of the experimental V–T_{in}. It is therefore essential to assess beforehand both the accuracy of this characteristic and the limits of applicability of the computational model, within which the search for the best fit is justified.

Concerning the first point we proceed as follows: (1) we identify a certain temperature cut-off T_{cut} below which the measured voltage is reasonably constant; (2) we compute the offset V_{off} in the voltage measurement as the average voltage $\langle V \rangle$ measured for $T_{in} < T_{cut}$; (3) we baseline (shift) the measured voltage $V \to V - \langle V \rangle$; (4) we assess the error of the computational fits (see below) only for measured $T_{in} > T_{cut}$. This procedure works reasonably for all cases of interest here except for shot 089-002, where V–T_{in} monotonically increases from 4.7 to 6.3 K (not shown) therefore not allowing finding a reasonable T_{cut}. For this reason the latter shot was excluded from our analysis.

The major limitation in the applicability of the M&M computational model to the case at hand comes from the assumption of uniform current distribution among strands, which is used in the code. Indeed, at least in the case of other similar conductors, e.g., the CSI, the current is *not* uniformly distributed, mainly because of the joints, at least below a certain threshold E_{cut} of maximum electric field measured along the cable [34]. In the case of the CSI, which has however a joint resistance over three times as high as the CSMC, analysis shows that E_{cut} can be around 10–15 μV/m at near maximum current and field [14]. Indeed, the current non-uniformity on the CSI, as shown by Hall probes [34], is probably associated with the unexpectedly high joint resistance (i.e. a significant portion of the cable, perhaps a whole petal, is not in proper contact with the joint surface), whereas there is no evidence of current non-uniformity at this level in the CSMC (in particular the joint resistance does not vary with time, as in the CSI [1]). Considering the lower joint resistance of the CSMC, we apply some reduction to the E_{cut} relevant for the CSI, and assume that in our case the current will be more-or-less uniformly distributed above $E_{cut} \sim 5$ μV/m (in view of the uncertainty on this figure, a limited sensitivity study to the value of E_{cut} will be performed below). This value of E_{cut} is probably conservative as it assumes the same non-uniformity level as the CSI (but with a lower resistance joint). Notice also that very recent calculations on the TFI [36], which has a joint resistance comparable to the CSMC, have shown that joint non-uniformity could not be responsible for the performance shortfall of this coil (despite previous speculations about manufacturing problems associated with the joints [37], there is no evidence of current non-uniformity in operation in this coil).

For each of the computational runs we then assess the voltage cut-off V_{cut} as the integral of the electric field computed along the cable when $\langle E \rangle$ reaches E_{cut} somewhere for the first time. The error of the computational fits is then assessed only for measured $V > V_{cut}$.

In order to assess the quality of the best fit for $T > T_{cut}$ and $V > V_{cut}$ we shall use here the following measure of the relative difference (error) between computed and measured voltage defined as

$$\sigma = \sqrt{1/N \sum [4(V_{comp} - V_{exp})^2/(V_{comp} + V_{exp})^2]}$$

where the sum runs over all (N) data points in the given time range.

Before entering the details of the analysis one last word is due on the possible error bars, which may affect the results of our best-fit search. Several causes can contribute to this error bar, among which: the best-fit search procedure itself (see below), the above-mentioned limited accuracy of the temperature profiles computed along the conductor by M&M, the uncertainties in the model limitations related, e.g., to the choice of V_{cut} and, last but not least, the uncertainties in the strand critical parameter values discussed previously. Below an attempt will be made to quantitatively assess most of these error-bar contributions.

5.1. Tests at 46 kA

We begin the detailed analysis by considering the evolution of the coil behaviour in the three tests performed at 46 kA. The measured V–T_{in} characteristics in shots 038-002 (year 2000), 020-002 (year 2001) and 090-002 (year 2002) are shown in Fig. 8 together with the computed evolution corresponding to the respective best-fit values of the parameters (n, ε_{extra}). The detailed features of the comparison are shown in Fig. 9, which is restricted to the voltage range $V > V_{cut}$, used for the evaluation of the fit error σ.

Notice that the simulation is capable in all cases to reproduce both the quantitative features of the charac-

[1] The time constant for current redistribution in a model coil cable from an inductive (and usually uniform) distribution after the current ramp up to a resistive (and possibly non-uniform distribution) is several thousands of seconds between petals, due to the wrappings [35]. The redistribution is often accompanied by a change in joint resistance [34] whose presence is a clear indication of non-uniform currents.

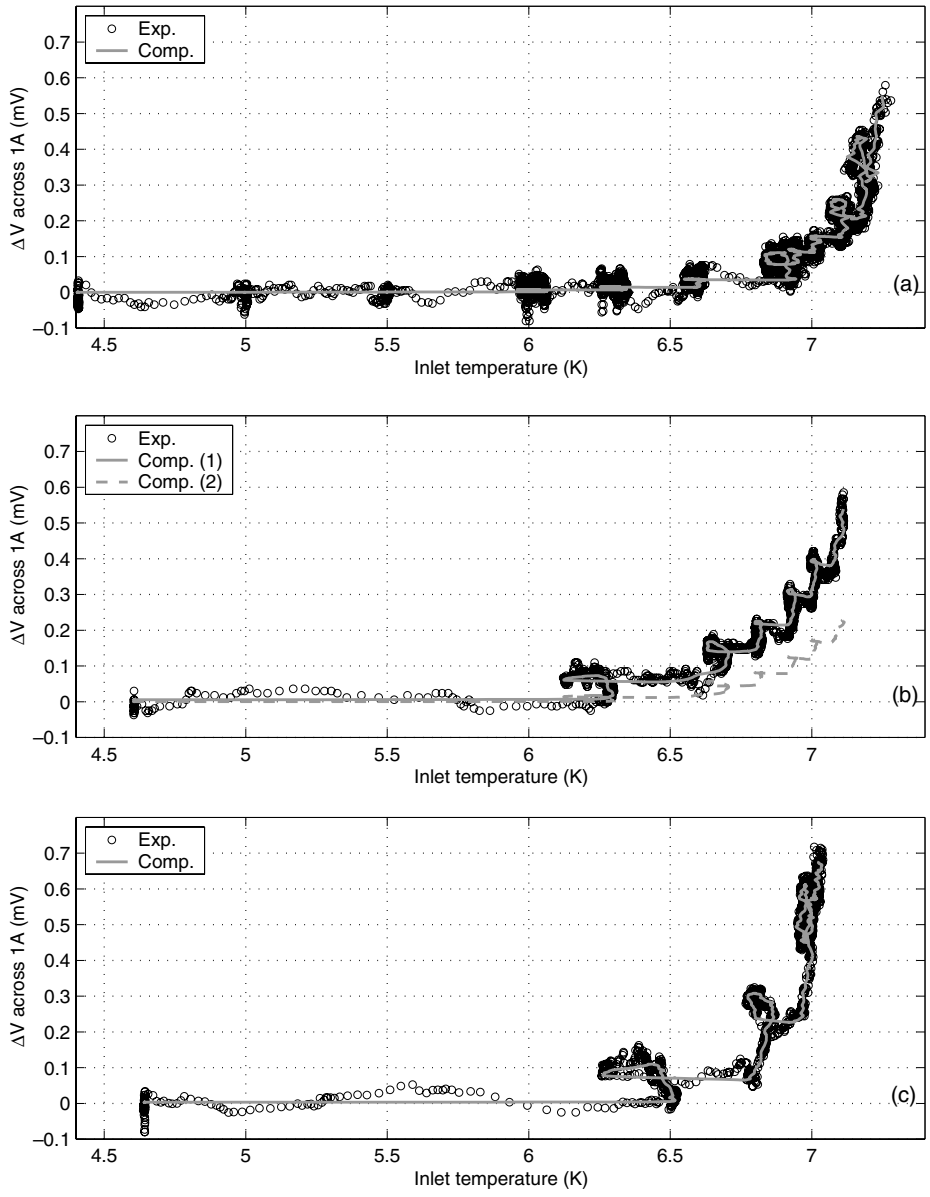

Fig. 8. Experimental (symbols) and computed (solid) evolution of the voltage drop across conductor 1A as a function of the inlet temperature @ 46 kA. From top to bottom: (a) shot # 038-002 (2000), best-fit parameters ($n = 9$, $\varepsilon_{\text{extra}} = -0.27\%$) and error $\sigma \sim 10\%$; (b) shot # 020-002 (2001), best-fit parameters ($n = 6$, $\varepsilon_{\text{extra}} = -0.30\%$) and error $\sigma \sim 8\%$; (c) shot # 090-002 (2002), best-fit parameters ($n = 7$, $\varepsilon_{\text{extra}} = -0.32\%$) and error $\sigma \sim 7\%$. The measured characteristics have been shifted by the value V_{off} as explained in the text. Only 1 every 5 experimental points is shown. The dashed line in plot (b) is computed using the same fitting parameters as used for plot (a).

teristic and also its qualitative features, e.g., the "loops". These are due to the wavy behaviour of the inlet temperature variation (see Fig. 7), which induces in turn a corresponding variation in the whole temperature profile and therefore in the resistive voltage.

It is also interesting to notice in Fig. 8b that if the best fit parameters of shot 038-002 were used also in this case, then they would predict a better performance than measured, whereas the best fit of the characteristic is found with a new pair of fitting parameters.

The computed spatial distribution of the strand temperature and of the electric field in the three shots at 46 kA, corresponding to the time when the critical electric field is first reached somewhere along the conductor, is shown in Fig. 10. Since the heat loss to the adjacent conductors is roughly balanced in this case by the strong Joule heating, the profile is almost flat so that, incidentally, $T_{\text{CS}} \sim T_{\text{in}} @ E = E_{\text{C}}$. The flat T profile results in an $\langle E \rangle$ profile, which more or less follows the magnetic field profile.

The results of our best-fit search at 46 kA are summarized in Table 3, together with those at other currents to be discussed below. In the table, the meaning of the ranges in n and $\varepsilon_{\text{extra}}$ is that they include the assessed

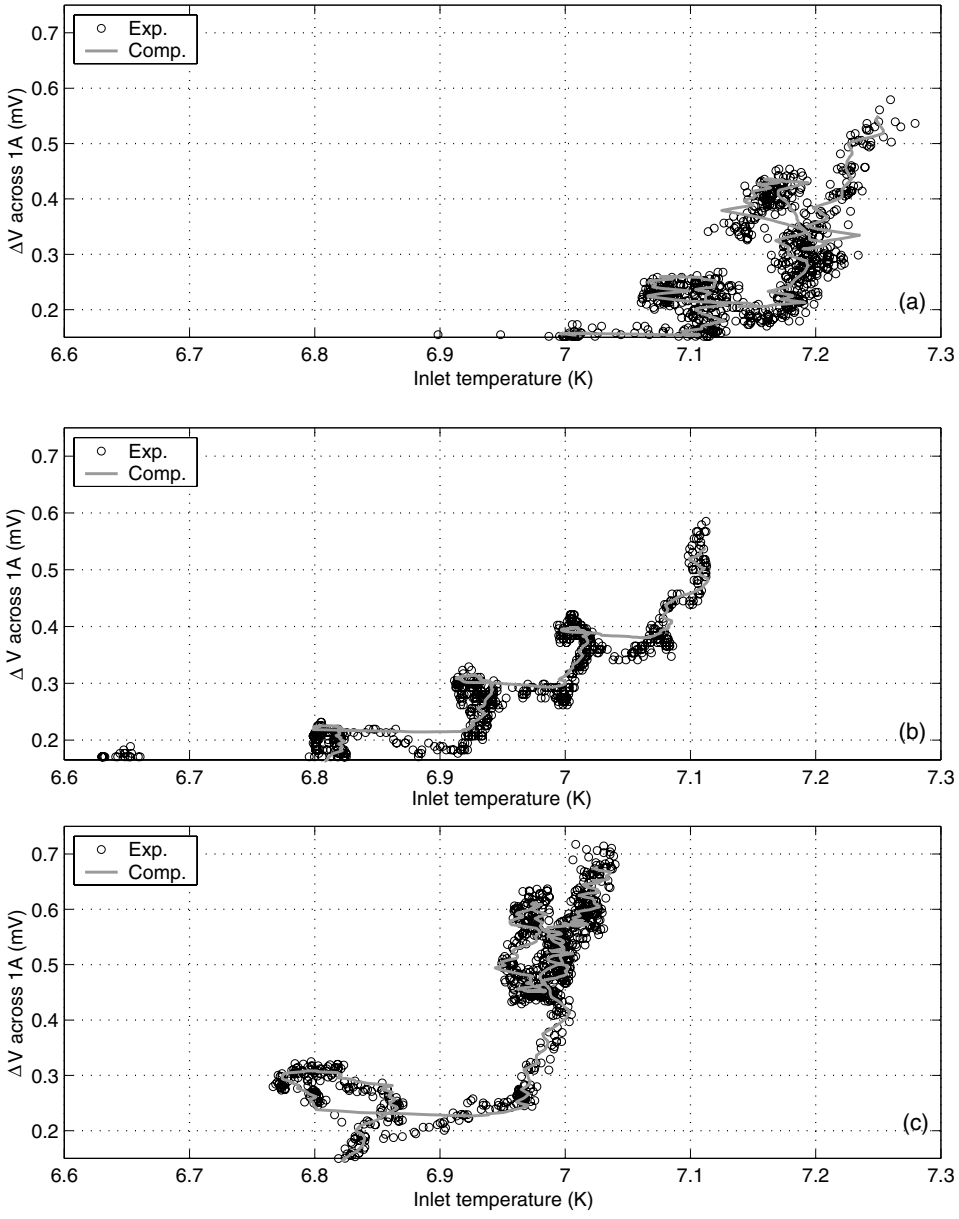

Fig. 9. Zoom on the late phase of the experimental (symbols) and computed (solid) evolution of the voltage drop across conductor 1A as a function of the inlet temperature @ 46 kA. From top to bottom: (a) shot # 038-002 (2000); (b) shot # 020-002 (2001); (c) shot # 090-002 (2002). The measured characteristics have been shifted by the value V_{off} as explained in the text. Voltage values are restricted to the range $V > V_{\text{cut}}$ (see text) where the error of the fit is computed, based on assumed uniform current distribution. Only 1 every 5 experimental points is shown.

contributions to the error bar. An impression of the error bar due to the best-fit search itself may be obtained from Fig. 11, where we plot for two relevant shots at 46 kA and at 30 kA the sensitivity of σ to small variations of $(n, \varepsilon_{\text{extra}})$, around the respective best-fit values. [2] The error bar due to the limited accuracy of the computed temperature profile may be estimated by modifying some of the input parameters (e.g., the heat transfer or the mass flow rate). This is done in such a way that the new computed $T_{\text{out}}^{\text{1A}}$ is on the opposite side of the measured value, with respect to the originally computed $T_{\text{out}}^{\text{1A}}$, by an amount roughly corresponding to the quoted ± 0.1 K accuracy of the temperature profile. Finally, sensitivity to the choice of V_{cut} turns out to be small.

Also two possible estimates of the experimental T_{CS} are given in Table 3: in the last column, we report the

[2] The fitting parameter values are accepted within this error bar if they lead to errors not larger than 50% of the minimum error. When no range is given, it means that within the search resolution, i.e., 0.01% for $\varepsilon_{\text{extra}}$ and 1 for n, the error was always larger than the minimum by more than 50%.

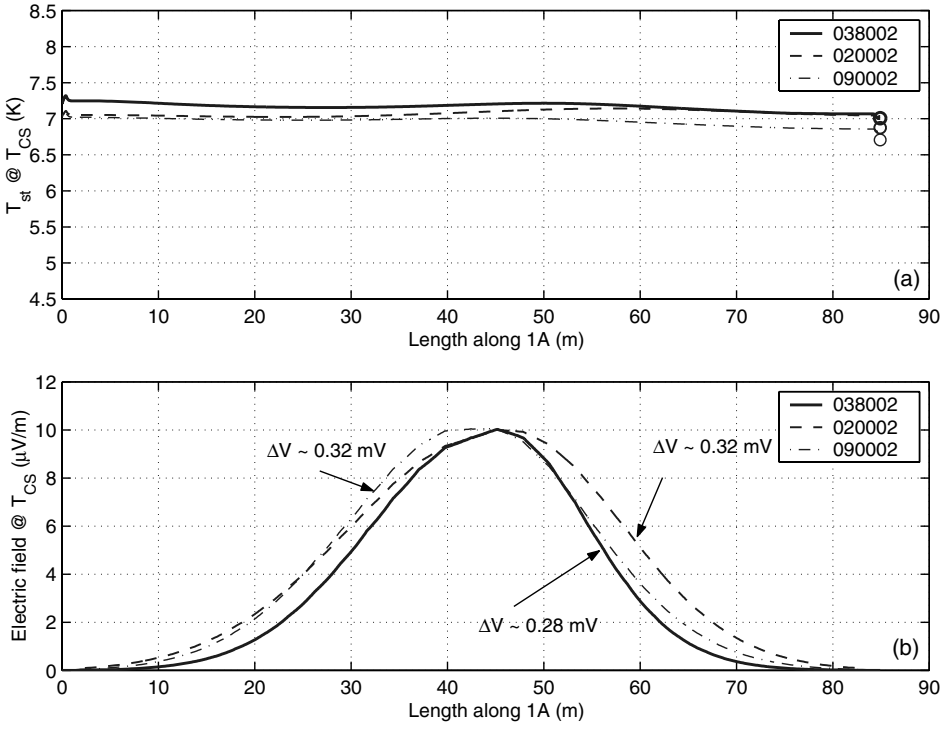

Fig. 10. Computed profile of strand temperature (a) and electric field (b) along conductor 1A when $\langle E \rangle = E_C$ is reached, for shot # 038-002 (2000); shot # 020-002 (2001); and shot # 090-002 (2002). In figure (a) the measured outlet helium temperature (open symbols) is also indicated as reference.

Table 3
Best-fit parameters (n, ε_{extra}) computed with M&M

Current (kA)	Shot #	V_{off} (μV)	T_{cut} (K)	V_{cut} (μV)	n	ε_{extra} (%)	T_{st}@10 μV/m (K)	x@10 μV/m (m)	T_{CS}@B_{max} (K)
46	038-002	49.6	6.1	150	7–10	−0.27 to −0.29	7.13–7.21	44.0–46.0	7.21–7.30
	020-002	–30.0	6.1	165	6–7	−0.30[a]	7.11	44.0–46.0	7.17
	090-002	4.7	6.1	150	7	−0.32 to −0.33	−6.96 to 7.01	39.0–45.5	7.03–7.08
40	041-002	28.4	7.5	160	6–9	−0.20 to −0.21[a]	8.72	42.5–45.5	8.78
30	051-002	42.4	11.5	90	4–8	−0.06 to 0.08	12.18–12.25	5.5–8.4	11.20–11.47
	092-002	29.4	11.5	70	4–6	0.08–0.16[a]	12.46–12.55	3.7–3.9	11.47–11.57
20	094-002	21.6	14	–	(8)	>0.06	–	–	

[a] The effect of accuracy of T profile was not assessed for this case.

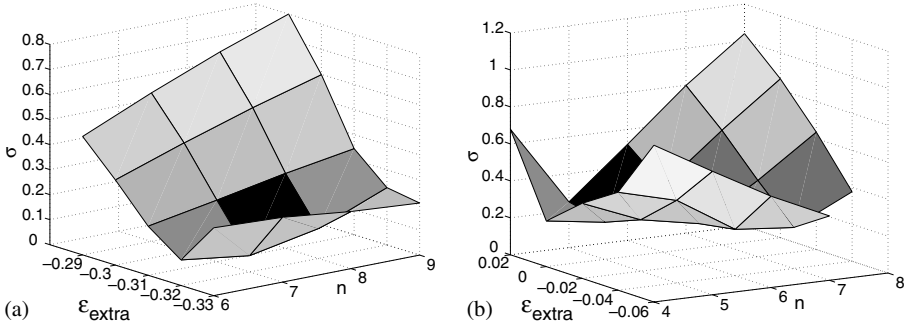

Fig. 11. Sensitivity of the simulation error to small variations of the fitting parameters (n, ε_{extra}) for shot # 090-002 at 46 kA (a) and shot # 051-002 at 30 kA (b).

values computed from Summers, using the best-fit critical parameters and the peak magnetic field for that current; in the previous column (recommended) we report the strand temperature at the time and location where the critical electric field $\langle E \rangle = E_C = 10$ μV/m is reached for the first time, together with the distance x from the conductor inlet to the corresponding location. The latter information obviously gives an indication of where the normal zone is being initiated, according to M&M, in the different cases.

Considering the shots @ 46 kA just presented, we may notice in Table 3 that there appears to be some tendency, although borderline, to need a decreasing ε_{extra} as operational cycles are accumulated in the coil, in order to explain the evolution of the coil performance. However, we cannot conclude if this is a real "fatigue-like" effect (in the sense of increasing degradation needed to reproduce the coil performance evolution with time).

5.2. Tests at 40, 30 and 20 kA

The comparison between computed (best fit) and measured V–T_{in} characteristics is shown in Fig. 12 for the single shot at 40 kA, and in Fig. 13 for the two shots at 30 kA. It may be noticed that, again, good quantitative and qualitative accuracy is obtained from the M&M simulations, albeit with somewhat increased errors.

The computed spatial distribution of the strand temperature and of the electric field in the two shots at 30 kA, corresponding to the time when the critical electric field is first reached somewhere along the conductor, is shown in Fig. 14. Compared to the case @ 46 kA (Fig. 10a), it is clear that the temperature profile is now much steeper. This is due to the combined effects of: increased heat transfer to the adjacent layers (because of the higher temperature difference), decreased Joule heating, and lower mass flow rate. Because of the steep $T(x)$, the T_{CS} is reached very near to the inlet (so that, again incidentally, $T_{CS} \sim T_{in} @ E = E_C$) and the electric field profile more or less follows the temperature profile. It should be noticed, however, that the normal zone is initiated possibly outside of the winding itself, i.e. in a region where the accuracy of the magnetic field map is rather low, thereby contributing an additional error bar in our assessment of the CSMC performance at low current.

Fig. 14 can be compared with Fig. 10 and Table 3 to illustrate another form of 'error' that can arise with the assessment of extra strain and n at low current. The part of the cable being assessed is clearly different at 30 kA from that at 40 and 46 kA (where in both cases the current sharing region is near the centre), and it has been subjected to a slightly different loading history (the $I \times B_{local}$ is about 15% lower than at the centre, for example). This can provide an explanation for small inconsistencies between the 30 kA data and the 40 and 46 kA data.

Several comments are due on the entries of Table 3 at currents below 46 kA. First of all, one can notice that the uncertainty on ε_{extra} increases at lower current, see also Fig. 11b, as a result of the fact that the strain sensitivity of the Summers scaling becomes smaller (i.e. in terms of temperature, the uncertainty is similar to that at high field but a bigger strain uncertainty is needed to account for it). However, despite the large spread of the ε_{extra} in the two runs at 30 kA, the corresponding difference in T_{CS} with respect to the average value is of only ±0.2 K.

Notice finally that for the test at 20 kA only a lower bound (computed with $n = 8$) is given for ε_{extra} since in that case, when the quench occurred and the coil current was dumped, the total voltage level was still rather low in 1A (essentially in the noise) and the T_{CS} criterion of $E = E_C = 10$ μV/m is far from being reached anywhere in the simulation of 1A.

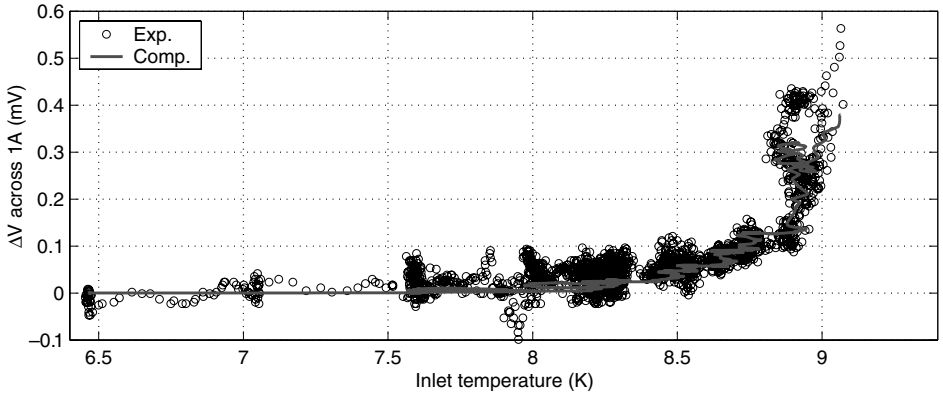

Fig. 12. Experimental (symbols) and computed (solid) evolution of the voltage drop across conductor 1A as a function of the inlet temperature @ 40 kA for shot # 041-002, best-fit parameters ($n = 8, \varepsilon_{extra} = -0.21\%$) and error $\sigma \sim 15\%$. The measured characteristics have been shifted by the value V_{off} as explained in the text.

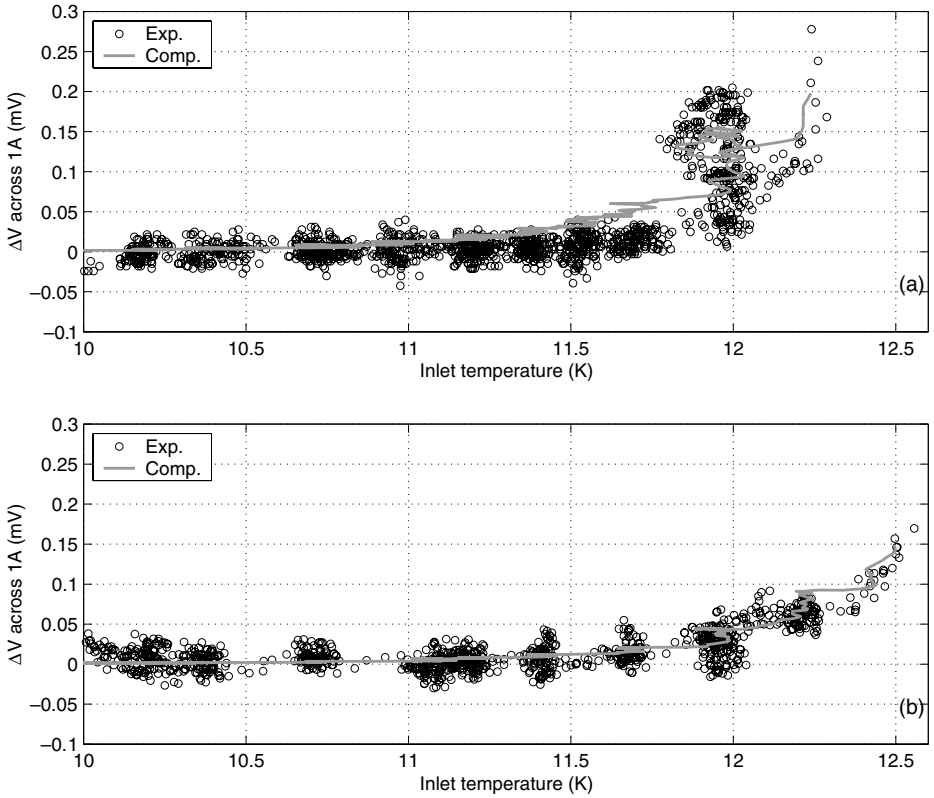

Fig. 13. Experimental (symbols) and computed (solid) evolution of the voltage drop across conductor 1A as a function of the inlet temperature @ 30 kA. From top to bottom: (a) shot # 051-002 (2000), best-fit parameters ($n = 5, \varepsilon_{\text{extra}} = 0\%$) and error $\sigma \sim 20\%$; (b) shot # 092-002 (2002), best-fit parameters ($n = 5, \varepsilon_{\text{extra}} = +0.10\%$) and error $\sigma \sim 9\%$. The measured characteristics have been shifted by the value V_{off} as explained in the text. Only 1 every 5 experimental points is shown.

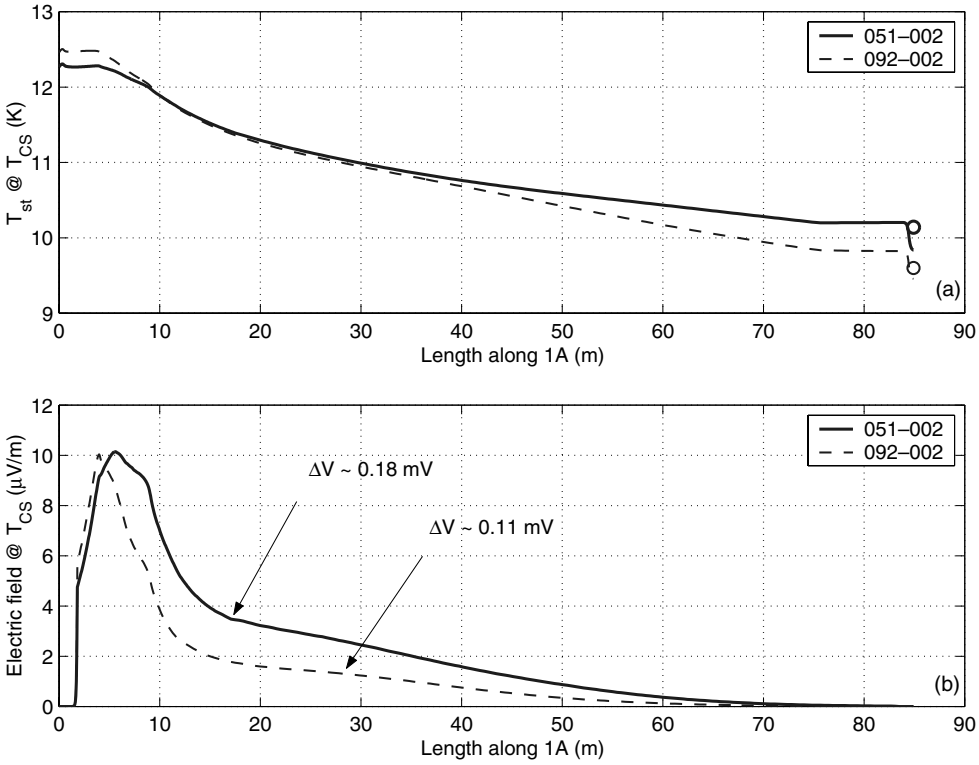

Fig. 14. Computed profile of strand temperature (a) and electric field (b) along conductor 1A when $\langle E \rangle = E_C$ is reached, for shot # 051-002 (2000) and shot # 092-002 (2002). In figure (a) the measured outlet helium temperature (open symbols) is also indicated as reference.

5.3. Test at 1 kA

A further measurement was performed at 1 kA (i.e. the minimum current where it is possible to detect a voltage transition, about 1 A/strand). The inlet temperature of the voltage runaway was 17.6 K, which suggests that the local temperature at the quench point was also quite close to 17.6 K, as there is very little scope for heat transfer effects in this measurement. An error of +0.1 K to −0.2 K could be reasonable (with the lower bound being slightly larger due to the temperature gradient along the conductor, due in turn to the temperature ramp).

The assessment of this test is complicated by several factors. Due to the high thermal gradients, the quench point is very close to the joint, probably not in the main winding but in the curved region leading in to it (see Fig. 6). The conductor performance in this region is not necessarily the same as in the main winding, as the operating loads are quite different (there is no applied tension and the transverse magnetic forces are much smaller). The field level at low current is uncertain, due to the presence of the Incoloy jacket. The local field due to the coil, at the joint, can be expected to be about 0.1 T, but then the Incoloy is no longer saturated and the ferromagnetic effect can result in significant local field changes (i.e. ±0.1 T). Since the quench point is very close to the joint, joint non-uniformity can have a significant impact. Finally, the strand data itself has to be obtained at low current, and the accuracy of the current measurement can have a significant impact on the interpretation of the data.

The impact of these factors is illustrated in Fig. 15, showing the Summers scaling for the CSMC strand compared to the measured strand point at low field [15]. The agreement here is very good, within about 0.1 K.

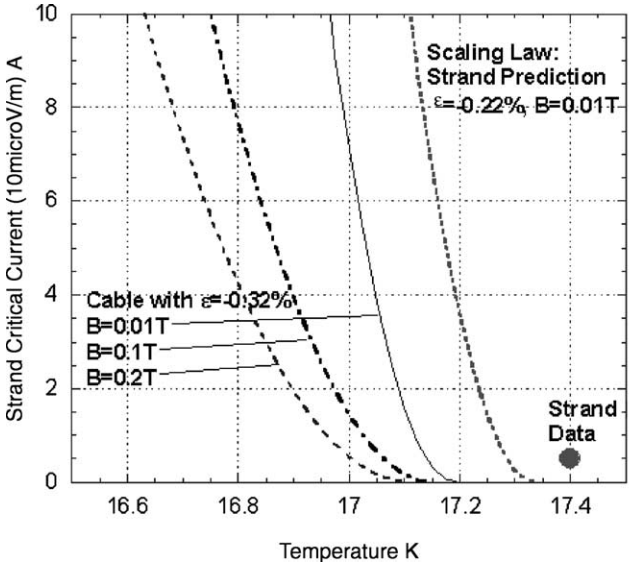

Fig. 15. Strand and coil measurements at low current and field. Strand parameters $T_{c0m} = 17.5$ K, $B_{c20m} = 32$ T, $C_0 = 0.74 \times 10^{10}$ A/m$^2\sqrt{\text{T}}$.

The scaling law predictions for the cable (thermal strain −0.32%) are also shown for three field levels. If the CSMC measurement result is 17.6 K (+0.1 to −0.2 K) at 0.9 A, then this seems rather above the level predicted by the scaling law although quite close to the strand data. One reason could be that the cable strain close to the joint is closer to the strand value than within the coil (due to slip out of the jacket at the joint). [3]

6. Discussion

The overall results of the CSMC layer 1A assessment are summarised in the two Figs. 16 and 17.

In Fig. 16 the extra strain deduced from the best-fitting of the voltage curves is plotted against $I \times B_{\text{local}}$. It shows quite clearly that the cable is performing less well than expected from the strand data, and that this degradation appears to scale with the mechanical load. Extrapolation of the linear least square fit to low currents (below 30 kA) has a fairly high error in view of the above-mentioned high error bars in the assessment of the 20 and 1 kA data.

In Fig. 17, the cable n deduced from the best-fitting of the voltage curves is shown superimposed on the plot of the measured strand n for various applied strains, as a function of critical current. It shows that the effective n of the cable is clearly below n_{strand} [19].

The most usual explanation for a performance shortfall in a short conductor or coil is a non-uniform current distribution arising at the joint. In the cable in conduit conductors the transverse resistance between strands is low but still sufficient in some situations to create a barrier to current redistribution, especially when the current non-uniformity is present to an extreme extent (e.g., a whole petal is not properly connected at the joint). Although current non-uniformity has not been specifically analysed in the CSMC layer 1A, extensive analysis [34,35] has been performed on the CSI, which has a very similar field distribution. This coil showed some clear non-uniform effects that could be verified by local field changes picked up by Hall probes installed on the conductor. As discussed earlier, non-uniform currents in the CSMC are expected to be limited to below a local electric field of ~5 μV/m (approximately 0.15 mV overall @ 46 kA), and this range has already been excluded from the analysis.

On the other hand, there is considerable additional evidence that mechanical effects are present in large cables and that these are capable of producing extra

[3] It is possible that the strand T_{c0m} is actually 17.6–17.7 K (rather than 17.5 K). This change would have a very small impact in the CSMC operating range but would improve agreement at low current, low field.

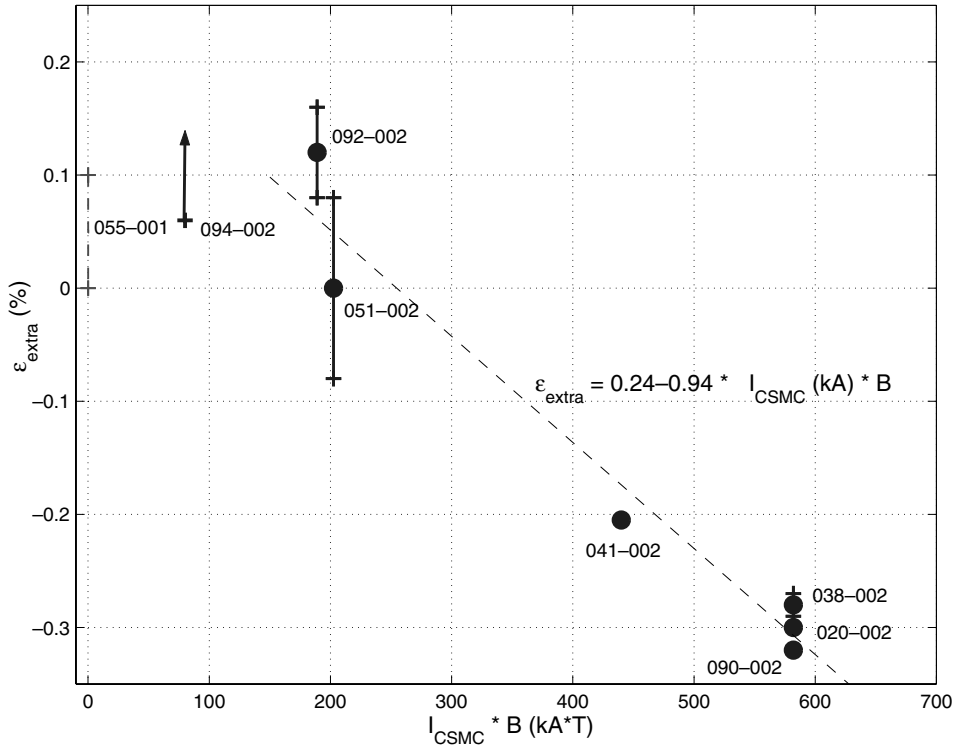

Fig. 16. Computed extra strain, from best fits of V–T_{in} characteristics, as a function of the product of CSMC transport current I times local magnetic field B (or, which is the same, of the force per unit length in kN/m), at the normal zone. The line represents a least square fit of the computed points, including a suitable distribution of the error inside the error bar. The error bars are discussed in the text.

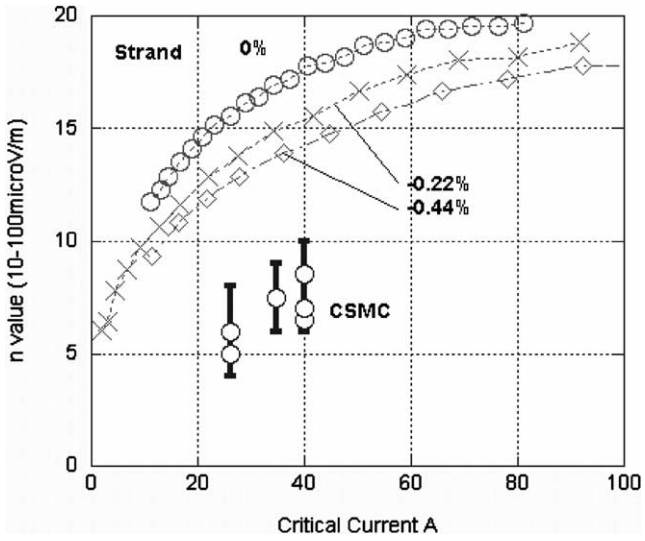

Fig. 17. n_{strand} (measured [17] at 10 and 100 μV/m) as a function of current, and its variation with applied strand strain, under uniform applied tension/compression at 8 K. Thermal strain at zero applied strain is −0.304% (arising from strand holder). Cable effective n for the CSMC layer 1A, as deduced from best fit of V–T_{in}, also shown.

strain. Measurements of short small cable samples with applied longitudinal strain show clearly that the cable responds both to thermal compression applied by the jacket and to externally applied longitudinal strain (which simulates the operational strain) [4]. In large cables (with over 1000 strands), cable movements in operation, associated with transverse magnetic loads, have been deduced using pressure drop measurements for the insert coils [32,38]. Mechanical analysis of strands in the cables [39] shows how the thermal compression, transverse magnetic loads and strand elasto-plasticity can all contribute to create longitudinal bending in the strands that can produce both a drop in strand current sharing performance and, due to inter-filament current transfer, a low n_{strand} [40]. Finally, destructive examination of the sub-size cables [41] has confirmed the permanent reduction of 'n' in strands from the high field regions as well as local wear effects from strand movements at the contact points.

Fig. 17 is further support for the suggestion that mechanical effects are the cause of the extra strain. The fact that the n of the cable deduced from the best fit is below n_{strand} at relatively high electric field (10 and 100 μV/m for the measured n_{strand}, 5–25 μV/m for the computed n of the cable) suggests that current non-uniformity cannot be the cause. These results are also consistent with cyclic inter-filament current transfer along the strands with a wavelength of a few mm. This is caused by the cyclic variation of longitudinal bending strain along strands in the cable due to the spacing of the inter-strand support points, as well as the cable twist [39]. Due to the plastic

deformation of the copper and bronze of the strands, the bending pattern is at least partially embedded into the strands after the first few load cycles. Removal of the magnetic loads would not generally be expected to lead to a recovery of n to the strand value. As discussed in [39,40], the drop in n due to current transfer between filaments is not expected to be directly proportional to the magnitude of the bending strain.

The existence of an 'extra' strain due to mechanical effects in the average strand assumed to be representative of the cable performance has not been quantified before, although it is not entirely unexpected given the size of the local magnetic loads on the strands and the possibility of load accumulation through the cable. It has not been considered in the ITER design criteria up to now, and its inclusion will obviously have a detrimental effect on the predicted performance of the ITER conductors. The CSMC layer 1A data is fairly accurate in the neighbourhood of the 46 kA, 13 T point but, due to the error in the assessment of the trend line, we would caution about extrapolating directly to cables which have a higher factor of field times current (which is the situation in, for example, the ITER TF coils where the field is 11.5 T and the current 68 kA [4]). The question also arises as to which extent changes in the cabling pattern and cable void fraction would change the assessment of this extra strain, as both could be expected to change the mechanical support of strands within the cable.

Finally, qualitatively similar conclusions (although quantitatively different, because of the different conductor type and winding, as well as operating conditions) could also be drawn from the recent M&M analysis of the Phase I TFMC T_{CS} tests [9,10]. Also there, an extra strain (scaling with the mechanical load) and a lower cable effective n than for the strand were needed, in order to reproduce the measured V–T_{in} characteristics at different transport currents.

7. Conclusions

A comprehensive if not exhaustive evaluation of the CSMC performance so far has been carried out, based on the results of T_{CS} tests of conductor 1A spanning over three years (2000–2002) and three experimental campaigns. The extensively validated M&M code was used, under the assumption of uniform strand properties and uniform current distribution among the strands, i.e., assuming that the coil performance can be analysed in terms of that of an "average" strand inside the coil. Critical parameters characterizing this average strand in terms of Summers scaling have been selected from a careful evaluation of the extensive strand database.

The strategy proposed here for the evaluation of the coil performance is based on the ability to reproduce with M&M the measured V–T_{in} characteristic, which relies in turn, as there are no sensors *inside* the coil, on the demonstrated ability of M&M to accurately reproduce (within ± 0.1 K) the measured temperature drop between inlet and outlet of the conductor. The major contributions to the error bars in the fitting parameters used have been either assessed computationally or based on error bars in the original experimental database.

While estimates of the T_{CS} at the different transport currents are obtained as a by-product of the analysis, our major results can be summarized as follows:

- An ad-hoc compressive contribution ε_{extra} to the average-strand longitudinal strain used in Summers is needed to reproduce the CSMC behaviour at 46 kA, indicating that the average strand in the coil performed less well than expected from the strand database.
- The ε_{extra} best fitting the V–T_{in} characteristic at the different transport currents scales with the mechanical load $I \times B_{local}$ at least in the range $30 \leqslant I \leqslant 46$ kA.
- The average-strand (or cable "effective") index n, needed to reproduce the CSMC behaviour in the same current range, lies significantly below the measured n_{strand}, at electric field conditions close or above T_{CS}.
- Considering also other measurements and analysis work on strands and cables, as well as the interpretation performed here, there seem to be strong indications that the mechanical load should be the most likely cause for the apparent performance degradation of the average strand in the CSMC.

Acknowledgements

The European Fusion Development Agreement partially financially supported the work of RZ and LSR, and LSR also benefited of a fellowship from ASP Torino. We should like to thank the whole JAERI-CSMC Test and Operation Groups for making the experimental campaigns of the CSMC and its insert coils a reality. RZ and LSR thank JAERI Naka, the Head of the Department of Fusion Engineering Research H. Tsuji, and the Head of the Superconducting Magnet Laboratory K. Okuno, for the kindest hospitality provided over the years: the feeling of friendship and collaboration that our Japanese colleagues have been able to establish was for us an essential ingredient for the success of our joint enterprise. Discussions with and help from many people, among which we should like to remember here K. Hamada, T. Isono, T. Kato, N. Koizumi, N. Martovetsky,

[4] This is obviously not the factor affecting the extrapolation of the present results to the ITER TF, which, e.g., should have a SS jacket as opposed to the Incoloy used for the CSMC conductor.

Ph. Michael, Y. Nunoya, M. Ricci, I. Rodin, M. Sugimoto, Y. Takahashi, M. Takayasu, are also gratefully acknowledged.

References

[1] Tsuji H et al. Conductor and joint development. Fusion Eng Des 2001;55(2–3):141–51.

[2] Tsuji H et al. Central Solenoid Model Coil. Fusion Eng Des 2001;55(2–3):153–70.

[3] ITER Final Design Report, July 2001, Design Requirements and Guidelines Level 1, Magnet Electrical and Superconducting Design Criteria, IAEA Vienna.

[4] Specking W, Duchateau J-L. First results of strain effects on critical current of Incoloy jacketed Nb_3Sn CICCs, MT15 Conference Proceedings, October 1997, Beijing, p. 1210.

[5] Savoldi L, Zanino R. M&M: multi-conductor Mithrandir code for the simulation of thermal-hydraulic transients in superconducting magnets. Cryogenics 2000;40:179–89.

[6] Savoldi L, Zanino R. Thermal-hydraulic analysis of T_{CS} measurement in conductor 1A of the ITER Central Solenoid Model Coil using the M&M code. Cryogenics 2000;40:593–604.

[7] Mitchell N. Assessment of the current sharing performance of layer 1A of the CSMC, April 2002, Private communication.

[8] Savoldi Richard L, Zanino R. The role of thermal-hydraulics in the ITER superconducting Central Solenoid Model Coil (CSMC) experiments. In: Proceedings of the 20th National Conference on Heat Transfer, 2002, p. 475–80.

[9] Zanino R, Savoldi Richard L, TFMC Testing Group. Performance evaluation of the ITER Toroidal Field Model Coil phase I. Part 1. Current sharing temperature measurement. Cryogenics, in press.

[10] Zanino R, Savoldi Richard L. Performance evaluation of the ITER Toroidal Field Model Coil phase I. Part 2. M&M analysis and interpretation. Cryogenics, in press.

[11] Zanino R, Martovetsky N, Savoldi L. Pretest analysis of T_{CS} measurements in the Central Solenoid Model Coil. In: Proceedings of the 18th International Cryogenic Engineering Conference, 2000, p. 195–8.

[12] Savoldi L, Michael P, Zanino R. Tests and simulation of thermal-hydraulic transients in the US Prototype joint sample. Int J Mod Phys B 2000;14:3183–8.

[13] Summers L, Guinan M, Miller J, Hahn P. A model for the prediction of Nb_3Sn critical current as a function of field, temperature, strain and radiation damage. IEEE Trans Mag 1991;27:2041–4.

[14] Knoopers HG, Nijhuis A, Krooshoop EJG, ten Kate HHJ, Bruzzone P, Lee PJ, et al. Third round of the ITER benchmark test. Inst Phys Conf 1997;158:1271.

[15] Godeke A, et al. Wide temperature and field scaling relations in Nb_3Sn ITER strands. University of Twente report UT-NET/EFDA 2000-5, September 2000.

[16] Martinez A, Duchateau JL. Field and temperature dependencies of critical current on industrial Nb_3Sn strands. Cryogenics 1997;37:865–75.

[17] Takigami H. Database of the CSMC conductors. JCT Internal Report, 19 Feburary 1999.

[18] Takayasu M, Childs RA, Randall RN, Jayakumar RJ, Minervini JV. ITER niobium–tin strands reacted under model coil heat-treatment conditions. IEEE Trans Appl Supercond 1999;9:644–7.

[19] Hampshire DP, Taylor DM. Characterisation of Nb_3Sn and Nb_3Al strands for model coils, University of Durham report DurSC0601, June 2001.

[20] Specking W, Duchateau JL, Decool P. Critical current vs strain tests on EU strands and subsize cable-in-conduit with stainless steel and Incoloy jackets. FZK Final Report GB5-M27 to ITER task no N11TT45, October 1997.

[21] Ekin JW. Strain Scaling law and the prediction of uniaxial and bending strain effects in multifilamentary superconductors. In: Suenaga M, Clark A, editors. Filamentary A15 Superconductors. New York: Plenum Press; 1980. ISBN 0-306-40622-5.

[22] Dalessandro J. Axisymmetric stress analysis of the ITER CS Model Coil for 13 T Lorentz loading with residual axial preload, Lockheed Martin Memo CSMC-MM-72, January 24, 1996; ITER CSMC Inner Module Design and Fabrication, Final Report, Rev 1, March 2000, MIT.

[23] Sugimoto M et al. Experimental results of cs Model Coil—mechanical performance in Japanese. Cryo Eng J Cryo Soc Jpn 2001;36(6):336.

[24] Zapretilina E. private communication.

[25] Verrechia M, Mitchell N. Impact of Incoloy in SULTAN conductor tests. CSMC and CS Coil, ITER internal memo, February 3, 2000 (unpublished).

[26] Zanino R, Carpaneto E, Portone A, Salpietro E, Savoldi L. Inductively driven transients in the CS Insert Coil (I): heater calibration and conductor stability tests and analysis. Adv Cryo Eng 2002;47:415–22.

[27] Savoldi L, Salpietro E, Zanino R. Inductively driven transients in the CS insert coil (II): quench tests and analysis. Adv Cryo Eng 2002;47:423–30.

[28] Zanino R, Savoldi Richard L, Zapretilina E. Modeling of thermal-hydraulic effects of AC losses in the Central Solenoid Insert Coil using the M&M code. IEEE Trans Appl Supercond, in press.

[29] Savoldi Richard L, Portone A, Zanino R. Tests and analysis of quench propagation in the ITER Toroidal Field Conductor Insert. IEEE Trans Appl Supercond, in press.

[30] Zanino R, Savoldi L. Tests and modeling of heat generation and heat exchange in the Full Size Joint Sample. In: Proceedings of the 18th International Cryogenic Engineering Conference (ICEC18), Mumbai, India, 21–25 February, 2000. p. 363–6.

[31] Zanino R, Santagati P, Savoldi L, Martinez A, Nicollet S. Friction factor correlation with application to the central cooling channel of cable-in-conduit super-conductors for fusion magnets. IEEE Trans Appl Supercond 2000;10:1066–9.

[32] Zanino R, Gung CY, Hamada K, Savoldi L. Pressure drop analysis in the CS Insert Coil. Adv Cryo Eng 2002;47:364–71.

[33] Hamada K, Kato T, Kawano K, Hara E, Ando T, Tsuji H, et al. Experimental results of pressure drop measurements in ITER CS Model Coil tests. Adv Cryo Eng 2002;47:407–14.

[34] Nijhuis A, Knoopers HG, et al. Effect of self-field and current non-uniformity on the voltage–temperature characteristic of the ITER Central Solenoid Insert Coil by numerical calculations. Cryogenics 2002;42:469–83.

[35] Mitchell N. Possible causes of the premature voltage gradient of the CS insert coil. IEEE Trans Appl Supercond 2002;12:1453–8.

[36] Zapretilina E. Progress Meeting with Efremov Lab., September 2002, private communication.

[37] Egorov S, Rodin I, Lantsetov A, Zapretilina E. TFCI DC test results and analysis, presented at the St Petersburg Workshop on the TFI, February 2002 (unpublished).

[38] Hamada K, Takahashi Y, et al. Electromagnetic force effect on pressure drop and coupling loss of cable in conduit conductor. Cryo Supercond, Cryo Eng J Jpn Cryo Soc (in Japanese), in press.

[39] Mitchell N. Mechanical and magnetic load effects in Nb_3Sn cable-in-conduit conductors. In: Paper Presented at the 2002 CHATS Workshop, Karlsruhe, Cryogenics, 2003; this issue. PII: S0011-2275(03)00043-2.

[40] Mitchell N. Analysis of the effect of Nb_3Sn strand bending on CICC superconductor performance. Cryogenics 2002;42:311–25.

[41] Bruzzone P, et al. The voltage/current characteristic (n index) of the cable-in-conduit conductors for fusion. In: Paper Presented at Applied Superconductivity Conference, Houston, 2002.